JMEPEG (2021) 30:4700–4711
https://doi.org/10.1007/s11665-021-05763-8

1059-9495/$19.00

Evaluation of the Hardening Behavior and Precipitation Kinetics of Precipitation Hardened 13-8+Mo Stainless Steel Using Avrami Relationships and a Global Fitting Procedure

Robert J. Hamlin and Charles V. Robino

Submitted: 2 January 2021 / Revised: 28 February 2021 / Accepted: 5 April 2021 / Published online: 4 May 2021

The purpose of the current investigation was to demonstrate the utility of the Avrami relationships and a global fitting procedure by applying it to precipitation hardened (PH) 13-8+Mo stainless steel (SS) hardness datasets taken from literature and calculating overall activation energies (Q_O) and growth constants (k_1 and n') for precipitation in this system. Additionally, this work evaluated assumptions concerning the significance of heat treatment hold times relative to heating and cooling cycles for short, welding-like, heat treatments using an additivity rule-based model. Data from four sources were evaluated using the global fitting procedure. These sources incorporated a significant range of PH 13-8+Mo SS chemical compositions, included both cast and wrought material, several solution treatment conditions, and a range of aging procedures. The method was applied to each dataset individually as well as all datasets combined and activation energies and growth constants were determined. All fits produced using this technique provided reasonable 1:1 correlations between measured and calculated hardness values. Application of this method to individual datasets produced k_1 values between $1.7e^3$ $sec^{-n'}$ and $2.0e^5 sec^{-n'}$, n' values between 0.40 and 0.57, and Q_O values between 150 kJ/mol and 199 kJ/mol. Application of this method to all the datasets combined produced k_1, n', and Q_O values of $8.7e^4$ $sec^{-n'}$, 0.38, and 234 kJ/mol, respectively. All values were in good agreement with values from literature for either lattice diffusion or dislocation pipe diffusion of the precipitating elements in PH 13-8+Mo SS. Further characterization is required to determine whether these values represent a fundamental significance. However, it was demonstrated that the global fitting procedure provides a reasonable and practical approximation of the hardening behavior for numerous PH 13-8+Mo SS datasets that have been exposed to a range of processing and heat treatment conditions.

Keywords Avrami, heat treatment, maraging, PH 13-8+Mo, precipitation kinetics, stainless steel

1. Introduction

Precipitation hardened (PH) 13-8+Mo stainless steel (SS) is a corrosion resistant martensitic stainless steel with high strength, moderate ductility, and low anisotropy making it ideal for applications in the military and aerospace industry. This alloy is strengthened during aging heat treatment by the formation of fine intermetallic β-NiAl precipitates. These precipitates form in the temperature range of 400°C to 600°C, are on the order of 2-3 nm in size, and are highly coherent with the martensitic matrix (Ref 1-5). Due to the small size, high coherency, and dislocation density in the martensitic matrix, these particles can be difficult to characterize, even if high-resolution transmission electron microscopy (TEM) is applied (Ref 2, 3). However, the low carbon content in PH 13-8+Mo SS results in a relatively ductile martensite and minimal carbide formation; thus, the strength in this alloy is primarily derived from the precipitate evolution. Therefore, the behavior and extent of precipitation is often interpreted by measuring mechanical properties such as hardness (Ref 4-7). In the current investigation the precipitation behavior in PH 13-8+Mo SS was evaluated using various hardness datasets in combination with classical precipitation kinetics relationships and a simple global fitting procedure.

Precipitation kinetics are often evaluated in PH stainless steels using the impinged volume Avrami relationship (Ref 4, 8-10):

$$x = 1 - \exp(-kt^n) \quad \text{(Eq 1)}$$

For which x is the fraction transformed, t is time and k and n are constants. In work performed by Robino et al. Ref 4 a relationship between hardness and volume fraction of precipitates was derived using hardening considerations, was combined with Eq (1), and was then applied to 13-8+Mo hardness data (Ref 4, 8-12):

$$\frac{H_t^{1.5} - H_0^{1.5}}{H_F^{1.5} - H_0^{1.5}} \propto x = 1 - \exp(-kt^n) \quad \text{(Eq 2)}$$

In Eq (2), H_t is the hardness after some time at a given temperature, H_0 is the solution treated hardness, and H_F is the peak aged hardness. This relationship was applied in combi-

Robert J. Hamlin, Formerly Lehigh University, 5E Packer Ave, Bethlehem, PA 18015; and **Charles V. Robino**, Formerly Sandia National Laboratories, Albuquerque, NM 87185. Contact e-mail: Roberthamlin184@gmail.com.

nation with the Arrhenius rate equation, Eq (3), to determine the apparent activation energy (Q) and the time exponent (n), for precipitation in this system (4).

$$\frac{1}{t} = k_0 \exp\left(-\frac{Q}{RT}\right) \quad \text{(Eq 3)}$$

In Eq (3), $1/t$ is the reciprocal of the time to reach a certain fraction transformed (and is an apparent rate to that fraction transformed), k_0 is a constant, Q is the apparent activation energy, R is the ideal gas constant and T is the absolute temperature (Ref 4, 7, 13, 14). Relationships similar to Eq (2) have been used to relate property measurements to precipitation behavior using this type of conventional Avrami-Arrhenius analysis and to determine values of Q and n for precipitation in various systems (Ref 4, 7, 13, 14). This information is useful for comparative purposes; however, practical application of these relationships to interpret precipitate evolution is difficult. The difficulty arises because these calculations depend on activation energies determined from apparent rates ($1/t$), which are determined for a specific fraction transformed. In reality the rates are constantly changing in a sigmoidal manner. Additionally, the fitting required for these calculations (i.e., plots of $\ln(\ln(1/1\text{-}x))$ versus $\ln(t)$ for various temperatures) often depends on a very limited number of data points for each temperature. This is due to the difficulty in obtaining property measurements within the short timescales required for precipitation at some temperatures in these systems. Thus, significant variability is observed when determining Q and n. Furthermore, averages of these values are typically applied, and can result in poor predictions (Ref 4, 7, 13, 14). In response to this, a more recent investigation performed by Hamlin et al. Ref 7 assessed the precipitation behavior in PH stainless steels 17-4 PH and PH 13-8+Mo using the Avrami-Arrhenius analysis in combination with a global fitting procedure, which allowed for analysis of all the hardening data at each temperature up to peak hardening simultaneously.

The previous investigation performed by Hamlin et al. Ref 7 evaluated two significantly different materials (PH 13-8+Mo SS and PH 17-4 SS) and demonstrated this method was applicable to both systems; however, because precipitate kinetics can be highly sensitive to changes in composition and processing methods, the focus of the current investigation is to evaluate the impact of these variations within one material system to demonstrate the effectiveness of this tool to capture the impact of these variations. Therefore, in the current investigation the global fitting procedure is applied to PH 13-8+Mo SS hardening data taken from various sources (Ref 2, 3, 7, 15). The data from these sources represent a wide range of material conditions (cast, forged, rolled), solution treatments, aging procedures (times ranging from 1 second to 16 hours and temperatures from 400°C to 625°C), and different concentrations of the precipitating elements. The fitting was applied to each dataset individually as well as the combined data to determine Avrami constants and activation energies. An additional goal of the current work is to test assumptions made in the previous investigation (Ref 7) concerning the significance of heat treatment hold times relative to heating and cooling cycles for short, welding-like, thermal cycles (i.e., isothermal versus non-isothermal heat treatments). A final goal is to further demonstrate the applicability of simple spreadsheet-based kinetic models for use in practical engineering assessments and heat treatment guides.

2. Materials and Methods

To apply the global fitting procedure described above, it is assumed that nucleation site saturation has occurred. This allows for the use of a simplified temperature dependence of k in the Avrami relationship. The assumption of site saturation is considered reasonable for this system based on its relatively rapid hardening, which indicates a negligible incubation period for precipitation and is further supported by the reasonable estimations that have been made using this assumption (Ref 4, 6, 7, 13, 14). Using this assumption, the temperature dependence of k is given by Christian Ref 16 in molar terms as:

$$\frac{dlnk}{d\left(\frac{1}{T}\right)} = \frac{n'Q'}{R} \quad \text{(Eq 4)}$$

where n' represents the value of n following nucleation saturation, and Q' is the activation energy associated with growth. In order to apply this relationship to a large set of experimental data simultaneously, an "overall" activation energy term, Q_O, was distinguished and used with Eq (4) to yield the integral expression for the temperature dependence of k, which is taken as:

$$k = k_1 \exp\left(\frac{-n'Q_o}{RT}\right) \quad \text{(Eq 5)}$$

where k_1 is a pre-exponential constant that differs from the Avrami k. Eq (5) can then be combined with Eq (1) using the same assumption of site saturation so that $n = n'$ in both expressions, which yields:

$$x = 1 - \exp\left(\left(-k_1 \exp\left(\frac{-n'Q_o}{RT}\right)\right)\left(t^{n'}\right)\right) \quad \text{(Eq 6)}$$

As described by Hamlin et al. Ref 7, Eq (6) can be used in conjunction with Eq (2) to determine k_1, Q_O, and n' using the least squares method and simultaneous iterative fitting of the three parameters using a spreadsheet solver routine. In the current investigation this method is applied to various PH 13-8+Mo SS datasets.

PH-13-8+Mo SS data from four sources were evaluated in this investigation. The reported chemical compositions for each dataset are shown in Table 1. These sources, along with the various material and thermal histories associated with each study, are shown in Table 2. Taken together, these studies incorporated a significant range of PH 13-8+Mo SS chemical compositions, included both cast and wrought material, several solution treatment conditions, and a range of aging procedures. Where required, the hardness reported in these studies was converted to Vickers hardness (HV) by using standard conversion tables (Ref 17).

3. Results and Discussion

3.1 Fits to Individual Data Sets

Using the global fitting method described by Hamlin et al. Ref 7 and summarized above, the hardness data from each of the four studies were initially fit on a study-by-study basis. That is, k_1, Q_O and n' were determined independently for data from each of the four sources. This analysis was performed

Table 1 Chemical compositions of PH 13-8+Mo SS reported for each dataset. All values in weight percent

Element	Hochanadel et al. Ref 3, Robino et al. Ref 4	Seetharaman et al. Ref 2	Hamlin et al. Ref 7	Asayama Ref 15
Fe	Bal.	Bal.	Bal.	Bal.
Cr	12.58	12.63	12.58	12.45
Ni	8.06	8.21	8.19	8.06
Mo	2.15	2.45	2.12	2.22
Al	1.06	0.8	1.04	1.08
C	0.027	0.04	0.04	0.036
Si	0.06	0.35	0.08	0.08
Cu	0.03	.	.	.
Co	0.01	.	.	.
Mn	0.01	0.45	0.04	0.04
Ti	0.01	.	.	.
P	0.005	0.05	0.005	0.010
S	0.001	0.03	0.001	0.005
N	0.002	.	0.002	.
O	0.0025	.	.	.

previously on the data from Robino et al. Ref 3 by Hamlin et al. Ref 7; however, this method is applied for the first time here to the data from Seetharaman et al. Ref 2 and Asayama Ref 15. Additionally, the fits for the Hamlin et al. Ref 7 data are different than those given in that reference. This is due to the fact that additional 900°C and 1200°C primary thermal cycle (PTC) data (Ref 18) are included here and were not incorporated in the fits in Reference 7. These fits are shown in Fig. 1, 2, 3 and 4 and include both the fraction transformed fits and the hardness estimates resulting from those fits. Additionally, examples of age hardening curves generated using the parameters are shown in Fig. 1(c) and 2(c). The fitted parameters k_1, Q_O and n' in Eq (6) for each of these fits are shown in figures and are summarized in Table 3.

For the fitting, the measured hardness values were first converted to fraction transformed using Eq (2). This approximation requires assignment of the initial and peak hardness, H_0 and H_F for each of the data sets. For these fits, the H_0 values were based on either the reported solution treated hardness or were estimated based on the minimum hardness reported for the lowest aging temperature and shortest time. H_F values were based on the peak hardness observed in each of the data sets. Overaged data from each source were not included in the fits since it must be treated separately by using an overaging model such as that described in Ref 19.

Fitting of the fraction transformed for each data set was accomplished in an Excel® spreadsheet by simultaneously varying the three parameters (k_1, Q_O, and n') using an iterative method embodied in the "Solver" subroutine. For these fits, the least squares method was used to minimize the residual difference between the measured and calculated fractions transformed. Following this minimization, the calculated fractions transformed were converted back to hardness using Eq (2). The Excel Solver settings were Generalized Reduced Gradient Nonlinear, central derivatives, with 1E-20 convergence and constraint precision. The fits were generally seeded with values obtained in Reference 7 and typically converged to a solution in a few seconds. Solutions were generally unique, and insensitive to the seeded values. However, the exception to this was the Asayama Ref 15 data which was somewhat sensitive to the seed values, and essentially equivalent fits (in terms of both R^2 and 1:1 correspondence) could be obtained over a range of k_1, Q_O and n' combinations. This range of parameter value combinations was generally similar to the range of values in Table 3, and the reduced sensitivity is thought to be due to the comparatively small number of data points in the Asayama Ref 15 dataset.

One assumption required to derive these parameters is that heat treatments are isothermal in nature and there is no hardening during heating and cooling. This could be viewed as problematic for the data obtained by Hamlin et al. Ref 7 since the heating and cooling portions of the thermal cycles used in their investigation were larger percentages of the overall thermal cycles. However, the parameters obtained using that data were comparable to the other parameters in Table 3, which suggests this assumption is reasonable for both long and short timescales. This assumption is evaluated in more detail using an additivity rule (Ref 16) based model in a subsequent section of this discussion.

The fits for each of the individual data sources are quite good, and result in acceptable 1:1 correlations. This information can be used to generate plots similar to Fig. 1(c) and 2(c) which show age hardening curves created using these parameters and also include the measured hardness data for comparison. Further, the generally good correlations for each of the materials imply that, for any given heat lot and application, a simple set of parameters can be developed to either define alternative heat treating conditions, or to "fine tune" standard PH 13-8+Mo SS heat treating conditions toward specific properties. Upon receipt of a new heat lot of material, a few selected aging trials over a range of time and temperature should be sufficient for reliable fitting. Note that, for a small data set some sensitivity to the seed parameters, such as that discussed above for the Asayama Ref 15 data, may be encountered. This should not limit the utility of the fits provided good correlations are obtained, and the seed parameters (especially n' and Q_O) are selected from within the range shown in Table 3 or are based on the parameters from the combined fitting discussed in the next section. In any case, the parameters developed from the aging trials can then be used to identify the heat treating characteristics and response of that heat and can then be used to define alternative heat treating conditions, or to "fine tune" standard heat treatments. Stated differently, from a practical standpoint this simple fitting

Table 2 Material and thermal histories

Source	Sample size and processing	Thermal history	Ni, Al, and C, wt.%
Hochanadel et al. Ref 3, Robino et al. Ref 4	Cast, machined to 10 mm x 10 mm x 4 mm	Solution treated at 927°C for 1.5 hours in molten salt pots, fan cooled and then refrigerated for 2 hours at − 72°C. Aged at 510°C, 538°C, 566°C, 593°C for times ranging from 60 seconds to 16 hours in high temperature molten salt pots.	Al: 1.06 Ni: 8.06 C: 0.027
Hamlin et al. Ref 7	Hot rolled to 8mm diameter	Solution treated at 927°C for 1 hour, water quenched, aged at 510°C, for 4 hours in open air convection furnaces. Heated in a Gleeble in air at 1000°Cs^{-1} to 900°C, 1100°C, or 1200°C, and cooled at ~100°Cs^{-1} as a primary thermal cycle (PTC). Then heated in a Gleeble at 1000°Cs^{-1} to 400°C, 500°C, 550°C, or 600°C and held for 0, 5, 60, and 120 seconds.	Al: 1.04 Ni: 8.19 C: 0.04
Seetharaman et al. [2]	Hot Forged Bar, machined to 3 mm thick samples and then cold rolled to 0.5 mm	Solution treated (ST) in helium 900°C or 1100°C for 30 min and water quenched, aged at temperatures between 425°C and 625°C for 1 or 4 hours.	Al: 0.8 Ni: 8.21 C: 0.04
Asayama Ref 15	20 mm diameter bar	Solution treated at 950°C for 30 min in neutral salt baths and water quenched. Aged in salt baths for 1 hour at temperatures ranging from 350°C to 500°C	Al: 1.08 Ni: 8.06 C: 0.036

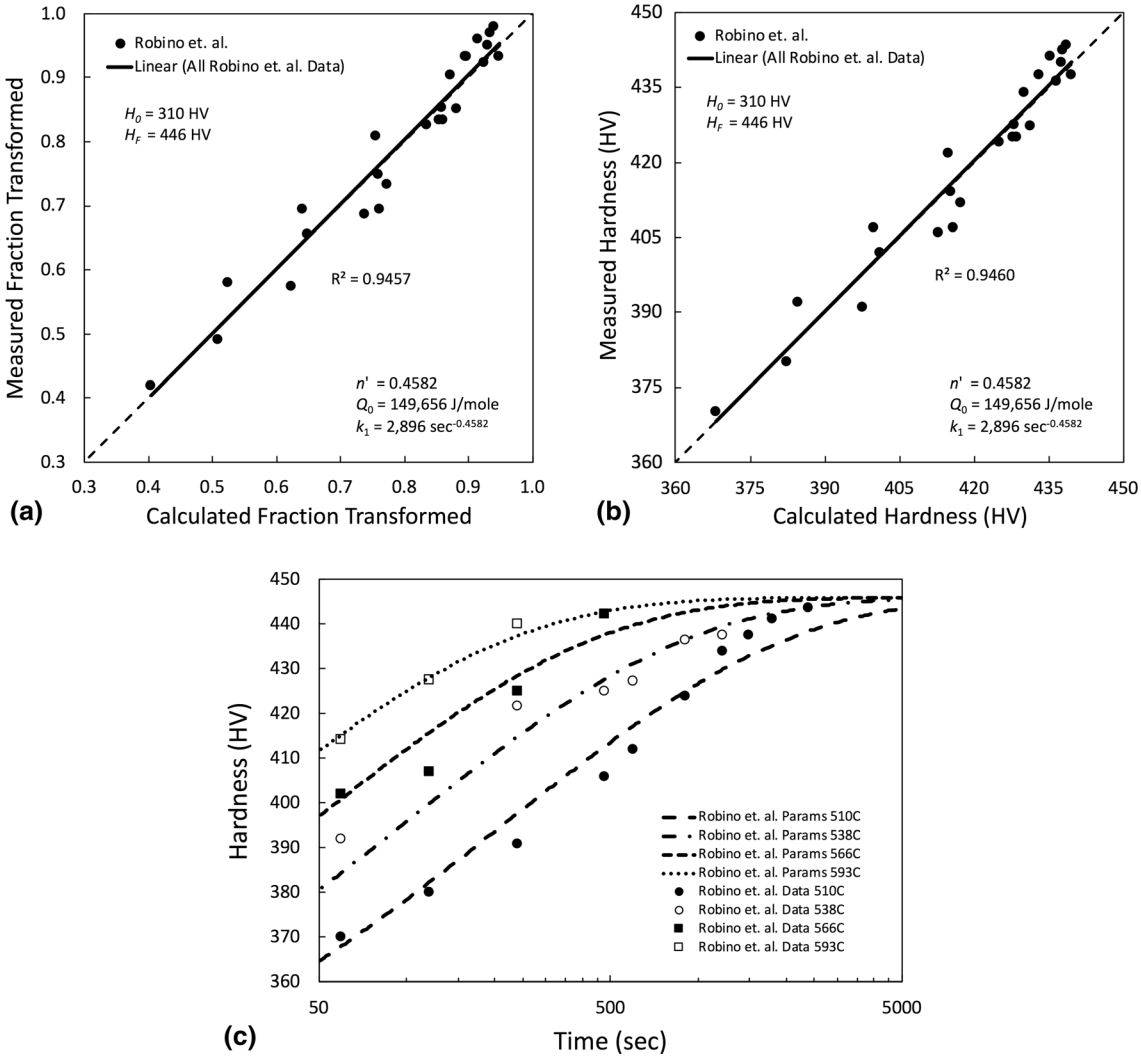

Fig. 1 Comparison of measured versus calculated (a) fraction transformed and (b) hardness for k_1, Q_O and n' fits to the Robino et al. Ref 4 data. The solid line is a linear fit to data and the dashed line is the 1:1 correlation line. (c) Original data and age hardening curves for the kinetic parameters shown in (a) and (b)

provides a useful formalism for the practicing engineer to assess heat treatment response using readily available desktop software and straightforward analyses. It is important to reiterate that the parameters in Table 3 do not apply to heat treatments in the overaging regime. It is also important to note that this method is not intended to preclude the development or use of, where available, more rigorous treatments of precipitation and hardening kinetics (see for example Ref 20 and 21).

The variability of the parameters in Table 3 is potentially due to the differences in processing conditions, thermal histories, and compositions for each material. These differences, which are summarized in Table 2, likely resulted in various grain sizes, dislocations densities, retained austenite contents, and carbide contents. Finer grain sizes, higher dislocation densities, lower retained austenite contents, and increased carbide contents could all contribute to higher hardness values and potentially affect the solution treated and peak aged hardness of each material (Ref 3, 12, 22). Additionally, reactions such as tempering (reduction in dislocations density), austenite reversion, and carbide formation are expected to some extent at the aging temperatures used in these investigations. As each of these reactions can influence the hardness and possess their own activation energy, they may contribute to the apparent activation energies calculated here. However, it should be noted that these competing reactions have been evaluated in other investigations and are thought to be minimal (Ref 3, 7). Hochanadel et al. (3) evaluated PH 13-8+Mo SS samples subjected to aging heat treatments using TEM. In their investigation they found negligible carbide formation and minimal reduction in dislocation density at the aging times and temperatures used in the current investigation (Ref 3). Furthermore, in the work performed by Hamlin et al. Ref 7 on PH 13-8+Mo SS, austenite formation during precipitation treatments was evaluated using XRD and found to have minimal impact on mechanical properties. The theory that competing reactions have minimal effect on the apparent activation energies calculated here is further supported by the comparable values calculated in Table 3. It should also be noted that supersaturation is one of the major driving forces for precipitation (Ref 23, 24). Therefore, variations in Al and Ni content may also impact the nucleation and growth rates

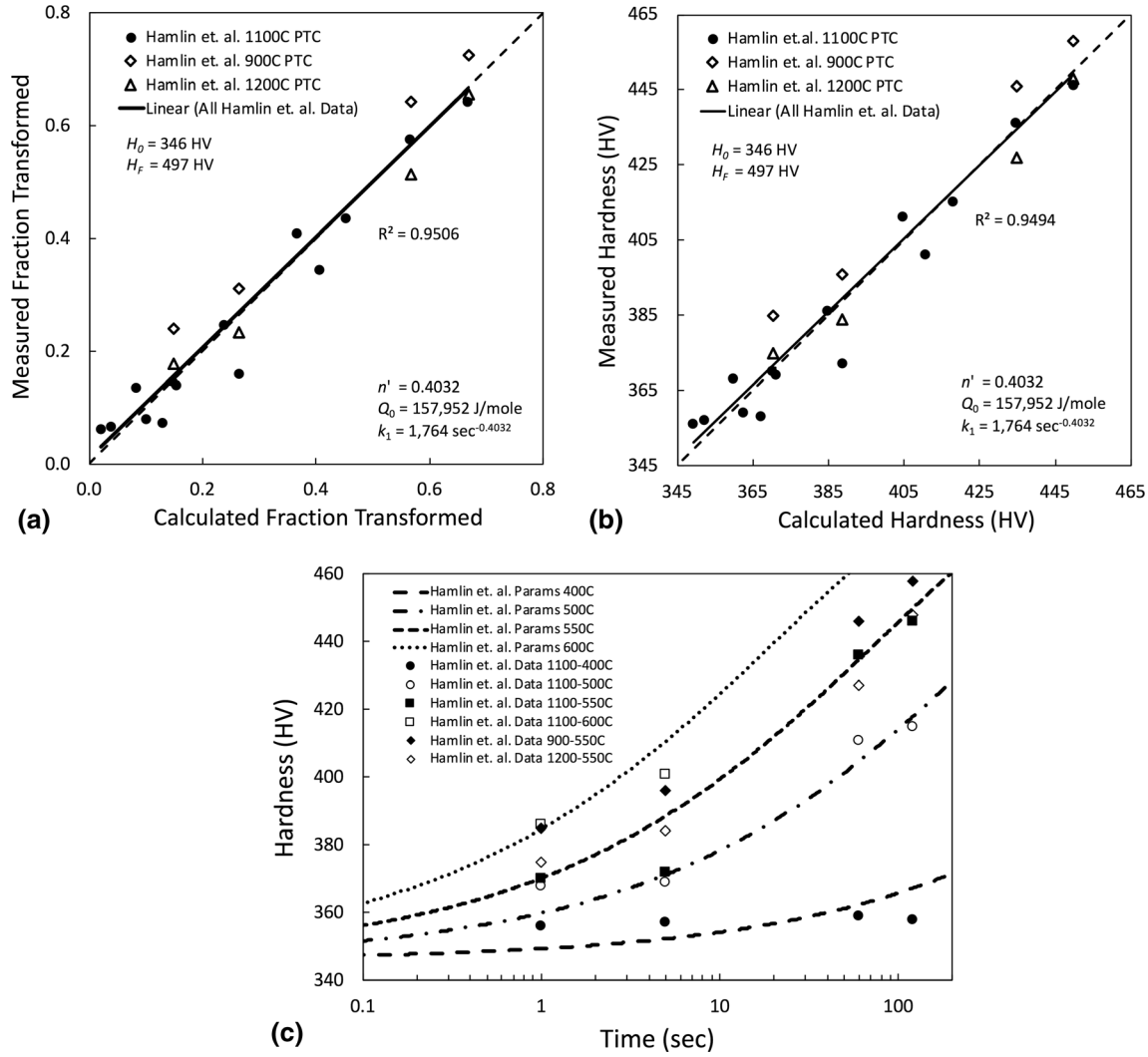

Fig. 2 Comparison of measured versus calculated (a) fraction transformed and (b) hardness for k_1, Q_O and n' fits to the Hamlin et al. Ref 7 data. The solid line is a linear fit to data and the dashed line is the 1:1 correlation line. (c) Original data and age hardening curves for the kinetic parameters shown in (a) and (b)

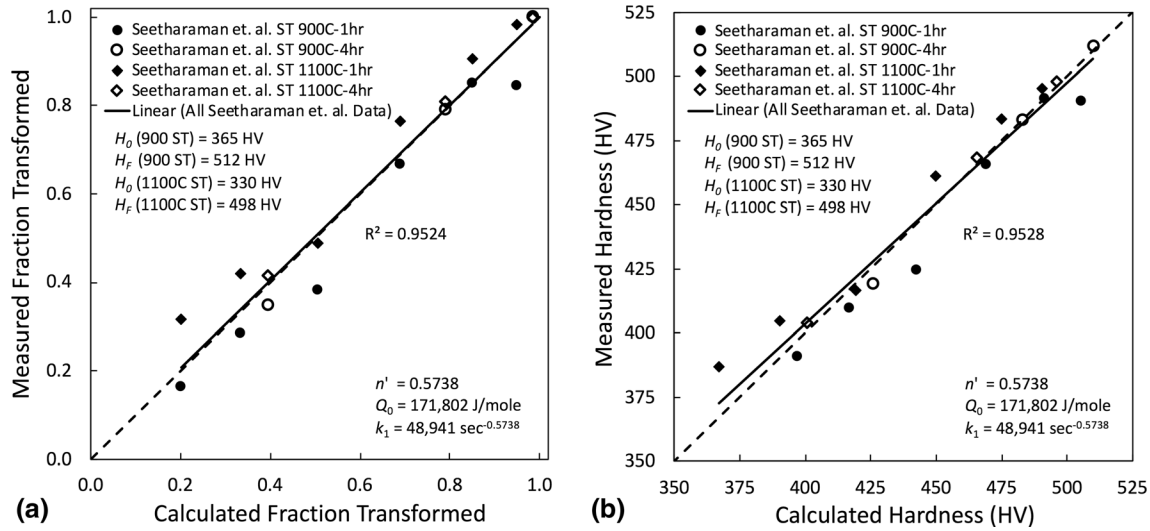

Fig. 3 Comparison of measured versus calculated (a) fraction transformed and (b) hardness for k_1, Q_O and n' fits to the Seetharaman et al. Ref 2 data. The solid line is a linear fit to data and the dashed line is the 1:1 correlation line

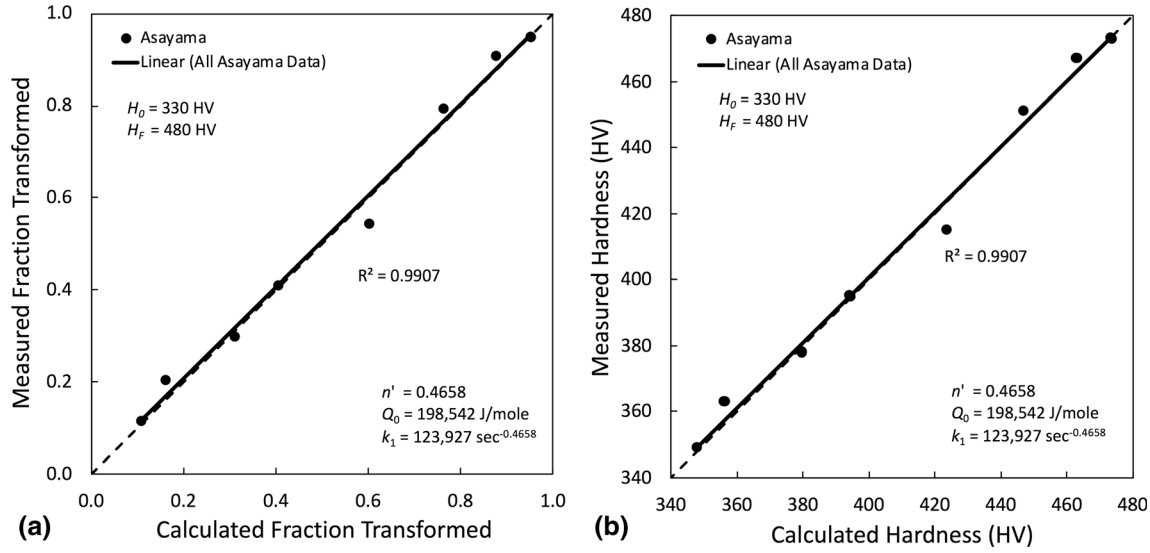

Fig. 4 Comparison of measured versus calculated (a) fraction transformed and (b) hardness for k_1, Q_O and n' fits to the Asayama Ref 1 data. The solid line is a linear fit to data and the dashed line is the 1:1 correlation line

Table 3 Constants and fit parameters for individual fits for the four data sources

Source	H_0, HV	H_F, HV	k_1, sec$^{-n'}$	Q_O, J/mole	n'
Robino et al. Ref 4	310	446	2,896	149,656	0.4582
Hamlin et al. Ref 7	346 (all PTC)	497 (all PTC)	1,764	157,952	0.4032
Seetharaman et al. Ref 2	365 (900°C ST) 330 (1100°C ST)	512 (900°C ST) 330 (1100°C ST)	48,941	171,802	0.5738
Asayama Ref 15	330	480	123,927	198,542	0.4658

observed in each system. Further discussion of this is provided below.

3.2 Fits to Combined Data Sets

Despite the variation in k_1, the Q_O and n' values in Table 3 are reasonably consistent. This suggests that combined fitting of all the available data might be feasible, and this was attempted as part of this study to further evaluate the utility of this method. The individual H_0 and H_F values for each heat shown in Table 3 were retained for this fitting. The results of the fitting are shown in Fig. 5, and the fitted parameter values are n' = 0.3813, Q_O = 234,236 J/mole, and k_1 = 87,131 sec$^{-0.3813}$. In contrast to what might intuitively be expected, the values for n' and Q_O do not fall within the range of the corresponding values that were determined from the individual fits (see Table 3). This is likely because the parameters were determined simultaneously rather than individually, and the fitting method is attempting to describe all the data from the four studies with a single set of parameters. However, as discussed further in the next section, it is important to note that the *transformation rates* calculated using the combined fit parameters generally fall within the *range of transformation rates* determined for the individual parameter fits.

Interestingly, the apparent activation energy value from the combined data fitting is higher than in any of the individual fits and is closer to that which might be expected on a theoretical basis. The activation energy for lattice diffusion of Al and Ni (the precipitating species) are 235 kJ/mole (56 kcal/mole) and 246 kJ/mole (59 kcal/mole), respectively, in α-Fe (25). As mentioned previously, the benefit of using the global fitting technique and evaluating all the data simultaneously is that a single set of parameters can be obtained for a given dataset consisting of multiple time and temperature exposures. This differs from the more conventional method of determining a different set of parameters for each aging temperature, using a limited number of data points, and then averaging the parameters. Moreover, the work performed by Hamlin et al. Ref 7 demonstrated that the parameters obtained using the global fitting procedure more accurately represented the hardening behavior in PH 13-8+Mo SS relative to the conventional method. Therefore, it is conceivable that by combining the datasets and further increasing the sample size, as shown in Fig. 5, the parameters begin to approach more fundamentally significant values for β-NiAl precipitation in PH 13-8+Mo SS. However, it is uncertain whether precipitation in PH 13-8+Mo SS and similar materials should be compared to theoretical activation energies for lattice diffusion of precipitating elements. Previous investigations have reported activation energies in the range of 100-150 kJ/mol for PH 13-8+Mo SS and similar materials, which were more consistent with the activation energy associated with enhanced dislocation pipe diffusion (Ref 4, 7, 13). In these investigations the lower activation energies were considered reasonable due to the high dislocation densities of the subject materials. Thus, relating apparent activation energies that are calculated in this manner to a physical phenomenon such as diffusion rates of an elemental species can be difficult (Ref 25). This is further

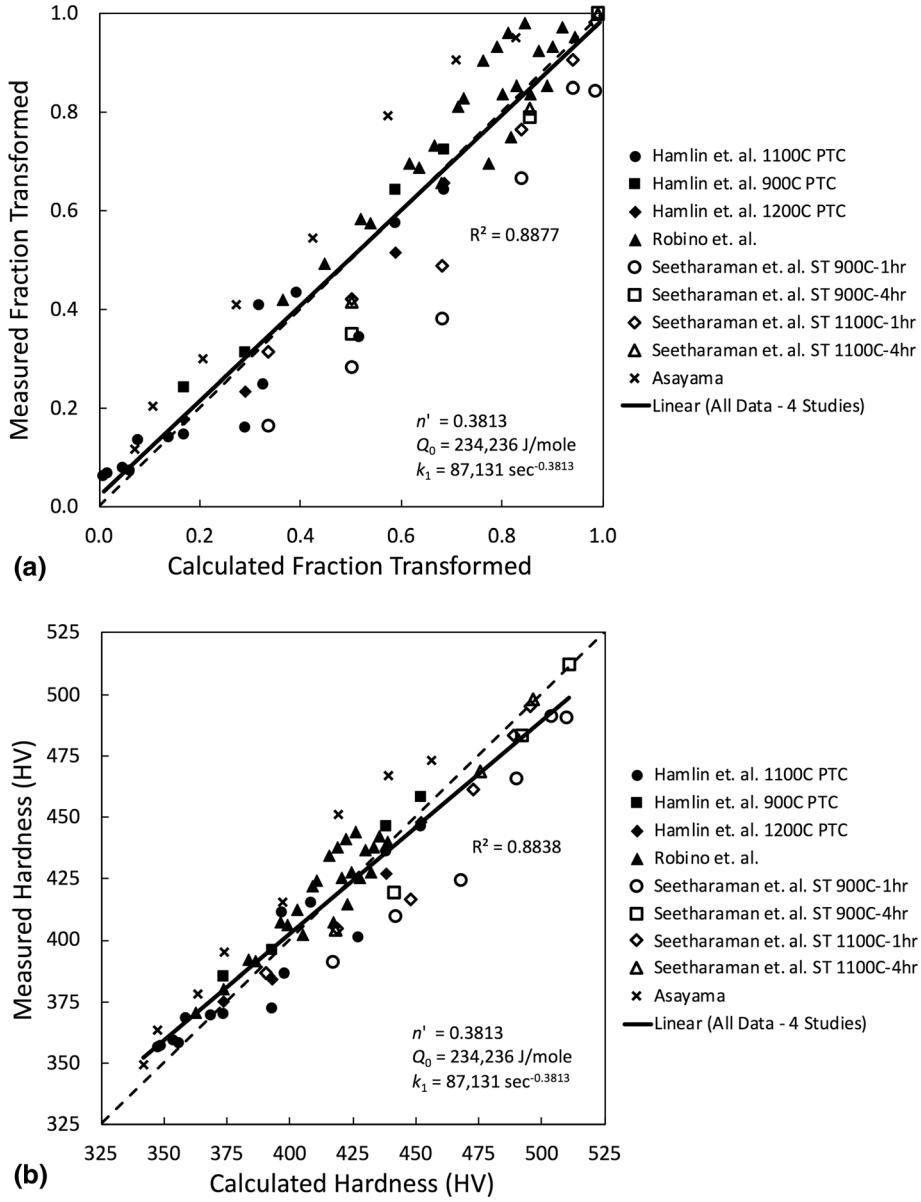

Fig. 5 Comparison of measured versus calculated (a) fraction transformed and (b) hardness for k_1, Q_O and n' fits to the four data sets of Table 1. The solid line is a linear fit to data and the dashed line is the 1:1 correlation line

illustrated by the work of Berkenpas et al. (Ref 26) which evaluated precipitation kinetics using similar methods. They concluded that these calculations are inaccurate when they depend on both mobility and driving force which each have their own activation energies. Furthermore, Starink (Ref 27) demonstrated that the apparent activation energy calculated using these techniques will vary with temperature and fraction transformed, when in reality the activation energy for a given process should be temperature independent. Therefore, even if the apparent activation energies appear reasonable, it is difficult to assign any fundamental significance to the values. However, as mentioned previously, the focus of the current investigation is not to develop a fundamental relationship for precipitation kinetics, but to provide a practical tool for interpreting the hardening behavior in PH 13-8+Mo SS. Furthermore, though these relationships may not directly represent a fundamental physical phenomenon, they can be used in combination with various characterization techniques to elucidate a more fundamental understanding of the kinetics in these systems.

In addition to evaluating the apparent activation energies, similar investigations have also attempted to relate the calculated n' values to precipitate growth habit (Ref 4, 7, 14, 16). The calculated values for n' in Table 3 and Fig. 5 ranged from 0.38 to 0.57. General guidance for n' given by Christian (Ref 16) is that values of 1/2 are typical for thickening of large plates, whereas 2/3 would be representative of the early stages of precipitation on dislocations. The values obtained here are slightly lower than expected for precipitation in PH 13-8+Mo SS which is believed to occur on dislocations (Ref 4). This discrepancy could be a consequence of using the global fitting procedure which determines the parameters based on data over the whole hardening range simultaneously, and thereby accounts for the entire range of fraction transformed values rather than just the early stages. Furthermore, as with activation

energy, n' is theoretically temperature independent, but has been observed to vary with temperature when calculated using indirect techniques such as hardness measurements (Ref 4, 7, 14). Therefore, the difference between the calculated and theoretical values could potentially be explained by the limitations of using indirect measurement techniques to estimate precipitation behavior. Regardless of whether the n' values determined here match well with theoretical values, they are in good agreement with those determined in other investigations which have used similar analysis methods on similar material systems (Ref 4, 7, 14). However, as stated previously, the focus of this investigation was not to relate these parameters to a fundamental mechanism of precipitation, but to develop a practical tool for evaluating the hardening behavior for a range PH 13-8+Mo SS samples. Although there is significant scatter, the 1:1 prediction lines observed in Fig. 5 are quite reasonable considering the wide range of chemical composition and processing conditions embodied in the four data sources. This implies that, in the absence of any specific heat lot information where more direct fits for the material of interest can be obtained (as described in the previous section), first-order estimates for non-standard heat treatments or heat treatment "fine tuning" should be reasonable using the fit parameters from the combined data sets.

3.3 Data Source to Data Source Variation

As mentioned previously, the All Data parameters did not fit entirely within the range of the parameters determined for each individual dataset (Table 3). This is because the parameters are not determined individually or by using an average, but rather by finding a best fit to the combined data sets. Therefore, rather than comparing individual values for each parameter, it is perhaps more appropriate to compare the various fits by using them (with Eq (6)) to calculate the time dependence of the fraction transformed. Plots of estimated fraction transformed as a function of time were constructed for various temperatures using the kinetic parameters obtained in the two previous sections. Examples of these plots for early times (shown in linear time) and long times (shown in log-time) for aging at 510°C are shown in Fig. 6. The plots in Fig. 6 indicate the rates are comparable for each dataset, with the exception of the precipitation kinetics reported by Seetharaman et al. Ref 2 which are considerably more sluggish. Observation of Table 2 indicates that the material evaluated in that work had significantly lower Al content than that of the other three studies. As mentioned previously, the lower Al content would result in a decreased level of supersaturation which is a driving force for precipitation and could potentially explain the sluggish kinetics observed in this dataset (Ref 23, 24). Supersaturation depends on concentration as well as the solubility limit of the matrix phase in which precipitation is occurring. In work performed by Hamlin and DuPont Ref 6 the solubility limit of Al in PH 13-8+Mo SS was calculated using ThermoCalc thermodynamic modeling software over the temperature ranges in which precipitation occurs in this alloy. It was apparent from their findings that increasing the Al concentration would not only increase the level of supersaturation at any given temperature in the aging regime, but would also increase the temperature range in which supersaturation existed and precipitation could occur (Ref 6).

Derivation of Eq (6) requires the assumption that nucleation site saturation has been achieved, and that only precipitate growth is associated with the hardening in the fitted data. This assumption is often considered reasonable in PH 13-8+Mo SS and similar systems based on the rapid rate of precipitation observed in these materials and is further supported by the reasonable estimations that have been made using this assumption (Ref 4, 6, 7, 13, 14). However, it is important to note that the indirect measurement technique applied in the current investigation cannot distinguish between the nucleation and growth regime of a precipitation reaction such as β-NiAl formation in PH 13-8+Mo SS. Nucleation rate is extremely sensitive to supersaturation (Ref 28). Thus, the decreased supersaturation in the Seetharaman et al. Ref 2 samples may have precluded site saturation. This would necessitate nucleation to occur during these experiments thereby decreasing the apparent growth rate. However, more in-depth characterization would be required to validate this.

In general, the rates and overall progress of the transformation determined using the All Data parameters, shown in Fig. 6, fall within the range determined for the individual data sets. However, this is not true at very short and very long times and is likely a consequence of the significantly slower kinetics observed in the Seetharaman et al. Ref 2 data. The slow kinetics of this dataset make it more difficult to obtain a global fit for the combined datasets, which decreases the R^2 value and forces an adjustment of the All Data parameters to compensate for the outlying data. This results in a "flattening" of the sigmoid associated with the All Data fit in comparison to the individual fits. Other possible contributions to this discrepancy include the fact that the Hamlin et al. Ref 7 data were determined using short times, whereas the other datasets were primarily determined at long times. Therefore, the rates determined above for individual datasets essentially require extrapolation at either short or long times. Nevertheless, regardless of this minor discrepancy, the All Data parameters provide a reasonable approximation of the transformation rate that is comparable to the rates determined for individual datasets.

3.4 Testing of Isothermal Assumptions for Hamlin et al. Ref 7 Data

In the prior work, an implicit assumption is that the fitted heat treatments are isothermal in nature. It is acknowledged that some amount of precipitation may occur during heating and cooling; however, for the majority of the four sources, the assumption is considered reasonable since the aging heat treatments were primarily on the order of 1 hour or longer. For the data from Hamlin et al. Ref 7, the aging heat treatments were conducted on a Gleeble for hold times as short as 1 sec. As a result, it is conceivable that the heat up and cool down times associated with those exposures may have contributed appreciably to the aging and were not accurately captured by the isothermal fitting. Therefore, the impact of the heating and cooling portions of these heat treatments were evaluated as part of the current investigation.

The simplest and most direct way to assess the contribution of the heat up and cooling times is to compare the effectively isothermal predictions from the (isothermal) Arrhenius/Avrami (AA) analysis above with predictions made by using a non-isothermal model with the same kinetic parameters. In the present work, this was accomplished by using an additivity rule (Ref 16) based model. The development of this model is similar to that discussed for overaging in Reference 18 and is referred to here as Arrhenius/Avrami/Additivity (AAA) analysis.

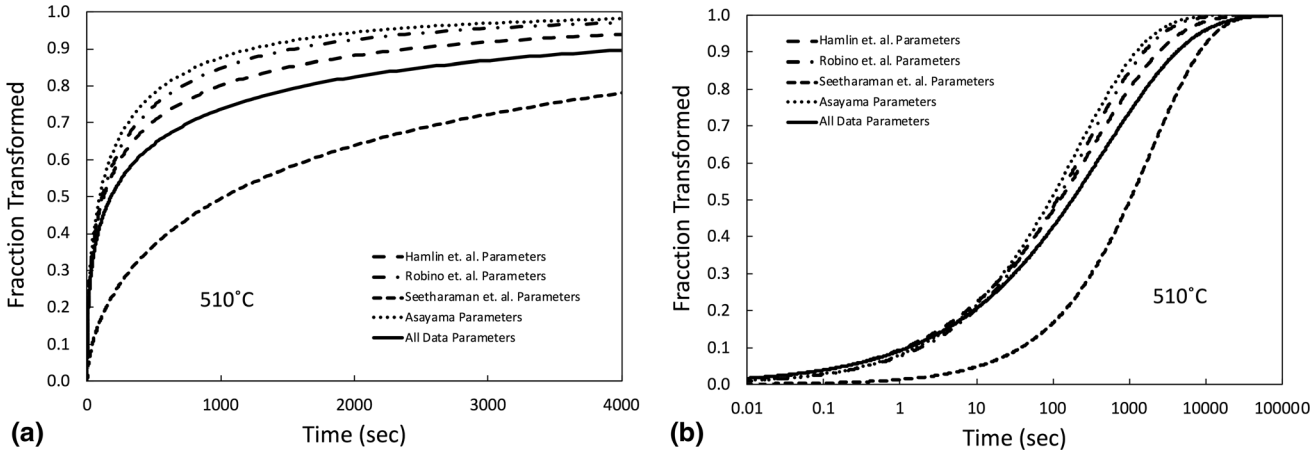

Fig. 6 Fraction transformed versus time at 510°C for the data from the various sources. (a) Early aging times. (b) Full transformation curves

The additivity rule as expressed by Christian Ref 16 is:

$$\int_0^t \frac{dt}{t_a(T)} = 1 \qquad \text{(Eq 7)}$$

where $t_a(T)$ is the isothermal time to reach a given fraction transformed and t is the time to that fraction transformed for the non-isothermal reaction. In terms of discrete time/temperature steps:

$$\sum_0^t \frac{\Delta t}{t_a(T)} = 1 \qquad \text{(Eq 8)}$$

Solving for t in Eq (6) yields:

$$t = t_a(T) = \left[\frac{\ln(1-x)}{-k_1 \exp\left(\frac{-n' Q_O}{RT}\right)}\right]^{1/n'} \qquad \text{(Eq 9)}$$

or, in terms of hardness, substituting for the fraction transformed, x, from Eq (2):

$$t_a(T) = \left[\frac{\ln\left(1 - \frac{H_t^{1.5} - H_0^{1.5}}{H_F^{1.5} - H_0^{1.5}}\right)}{-k_1 \exp\left(\frac{-n' Q_O}{RT}\right)}\right]^{1/n'} \qquad \text{(Eq 10)}$$

In keeping with the goal of identifying simple spreadsheet-based methods for routine desktop analysis, Eq (8) can readily be solved by using a goal seeking tool in any spreadsheet application. For example, a matrix similar to that shown in Table 4 can be constructed by dividing the thermal cycle into a series of short isothermal segments using the rectangular rule of integration (note that the Gleeble data of Reference 7, and most digital temperature cycle recording devices, is already in this form). For any given timestep, the only unknown in Eq (10) is the final hardness, H_t, and this is set as an adjustable parameter in the $t_a(T)$ column of cells. A goal seeking tool is then used to find the value for H_t that results in a SUM($\Delta t/t_a(T)$) value of unity.

The hardness resulting from the actual Gleeble thermal cycles used by Hamlin et al. (7) was estimated with this method. The results are compared with those determined using the isothermal assumption (Fig. 2) and are shown in Fig. 7. For these estimates, the parameters k_1, Q_O and n' from both Table 3 for the Hamlin et al. Ref 7 data and the All Data fits in Fig. 5 were used. These are referred to as Hamlin *et. al.* parameters and All Data parameters, respectively. Both parameter sets were evaluated in order to reduce any concerns that use of parameters derived from the Hamlin et al. Ref 7 data using isothermal AA analysis in the AAA analysis might constitute a circular argument.

The AAA estimates were within 8 HV of the AA estimates for both parameter sets, except for the 1100/600/1 predictions which were 16.7 HV different for both parameter sets. The AAA estimates are consistently similar to or higher than the AA estimates, while the deviations between the estimates are greatest for the shortest time thermal cycles and are most pronounced for the highest temperature cycles. This is illustrated graphically in Fig. 8 and is to be expected since the contribution to aging from the heat up and cool down cycles is most pronounced at these extremes.

The results in Fig. 7 and 8 demonstrate that the hardening contributions from the heating and cooling portions of thermal cycles with relatively short isothermal holds is not negligible. However, the differences in calculated hardness resulted in only minor variations in fits using two different sets of parameters. Therefore, the assumption that the fitted heat treatments are isothermal in nature is not unreasonable and is necessary to facilitate the calculation of initial parameters using simple spreadsheet methods. It is also worth noting that significant differences in calculated hardness were only observed when the combined duration of the heating and cooling portions of the thermal cycle was comparable to the length of the isothermal hold time. This further supports the assumption that the heat treatments were isothermal for the other data sources evaluated here as the isothermal hold times were significantly longer than the heating and cooling times in those investigations.

4. Conclusions

Avrami kinetics relationships and a simple global fitting procedure were applied to various PH 13-8+Mo SS hardness datasets to determine apparent activation energies and growth constants for precipitation. The hardness datasets used in this investigation were taken from various sources and included wrought as well as cast material, several solution treatment conditions, and a range of aging procedures. The fitting procedure was applied to each data set individually and to all

Table 4 Spreadsheet method for additivity determination of hardness resulting from a thermal cycle

Time, t	Temperature, T	Δt	t_a, T	$\Delta t/t_a$, T
t_1	T_1	t_1-0	Eq [10] using t_1 & T_1 with H_t as adjustable cell	$\Delta t_1/t_a(T)_1$
t_2	T_2	t_2-t_1	Eq [10] using t_2 & T_2 with H_t as adjustable cell	$\Delta t_2/t_a(T)_2$
t_3	T_3	t_3-t_2	Eq [10] using t_3 & T_3 with H_t as adjustable cell	$\Delta t_3/t_a(T)_3$
…	…	…	…	…
…	…	…	…	…
t_N	T_N	t_N-$t_{(N-1)}$	Eq [10] using t_N & T_N with H_t as adjustable cell	$\Delta t_N/t_a(T)_N$ = SUM($\Delta t/t_a(T)$)

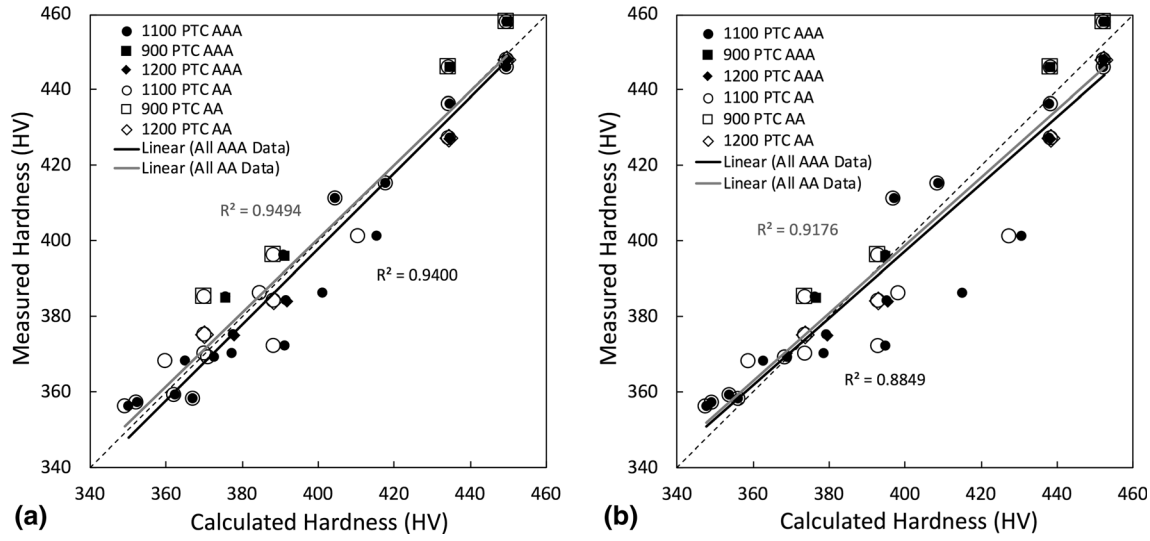

Fig. 7 Comparison of AAA and AA hardness estimates for Hamlin et al. Ref 7 data (a) Hamlin et. al. parameters, and (b) All Data parameters. AAA estimates are essentially coincident with, or are horizontally to the left of, the corresponding AA estimate. Solid black lines are linear fits to the AAA estimates and the solid gray lines are linear fits to the AA estimates

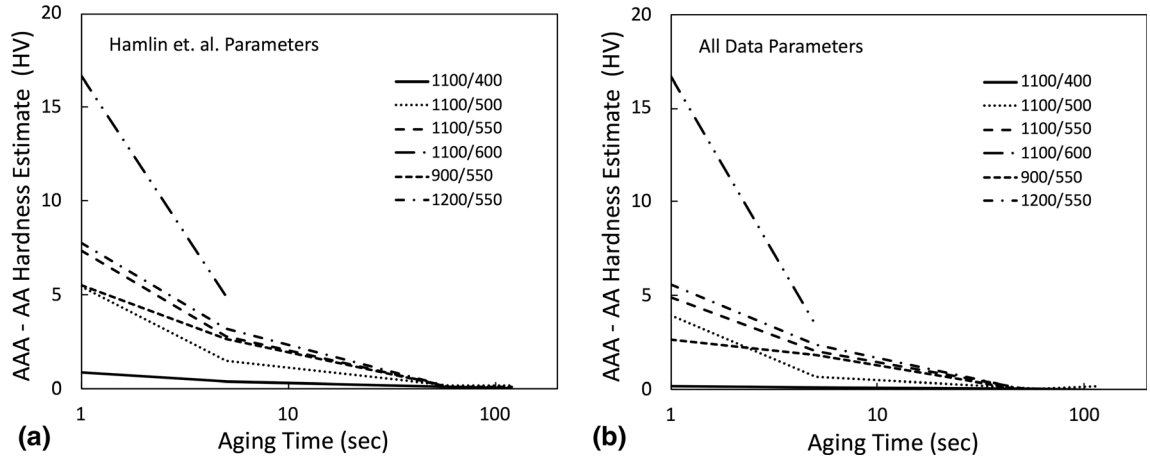

Fig. 8 Deviation between AAA and AA hardness estimates for Hamlin et al. Ref 7 data as a function of aging time for (a) Hamlin et al. parameters, and (b) all data parameters

datasets simultaneously to evaluate the utility of this method over a range of PH 13-8+Mo SS conditions. Additionally, an additivity rule-based model was applied to thermal cycle data from a previous investigation to test assumptions made about the effect of heat up and cool down times on the hardening response. The following conclusions can be drawn from this investigation.

1. Application of the global fitting procedure to individual datasets produced k_1 values between 1.7e^3 sec$^{-n'}$ to 2.0e^5

$\sec^{-n'}$, n' values between 0.40 to 0.57, and Q_O values between 150 kJ/mol to 199 kJ/mol.

2. Application of the global fitting procedure to all of the datasets combined produced k_1, n', and Q_O values of $8.7e^4$ $\sec^{-n'}$, 0.38, and 234 kJ/mol, respectively. These values may serve as reasonable seed values for future application of this method to additional PH 13-8+Mo SS datasets
3. Activation energies determined using this method were in good agreement with values from literature for either lattice diffusion or dislocation pipe diffusion of the precipitating elements in PH 13-8+Mo SS.
4. Fitting applied to each dataset and all of the datasets combined provided reasonable 1:1 correlations between measured and calculated hardness values with R^2 values ranging from 0.88 to 0.99.
5. Calculated transformation rates were comparable for each dataset except for one which had significantly lower aluminum content. The lower aluminum content conceivably resulted in decreased supersaturation and may have decreased the driving force for precipitation to occur, thereby slowing the apparent rate.
6. The additivity rule based model applied in this investigation demonstrated that the heating and cooling portions of thermal cycles with very short peak temperature hold times were not negligible. However, the differences in calculated hardness and fit observed with and without application of the additivity rule were minor. Therefore, the assumption that the heat treatments in the Hamlin et. al. [7] data are isothermal in nature is considered reasonable.
7. The Global fitting procedure applied in this investigation provides a reasonable and practical approximation of the hardening behavior for numerous PH 13-8+Mo SS datasets that have been exposed to a range of processing and heat treatment conditions.

Conflict of interest

On behalf of all authors, the corresponding author states that there is no conflict of interest.

References

1. J.A. Brooks and W.M. Garrison Jr., Weld Microstructure Development and Properties of Precipitation-Strengthened Martensitic Stainless Steels, *Weld. J. (Miami)*, 1999, **78**, p 280–291
2. V. Seetharaman, M. Sundararaman and R. Krishnan, Precipitation Hardening in a PH 13-8+Mo Stainless Steel, *Mater. Sci. Eng.*, 1981, **47**, p 1–11
3. P.W. Hochanadel, G.R. Edwards, C.V. Robino and M.J. Cieslak, Heat Treatment of Investment Cast PH 13–8 Mo Stainless Steel: Part I. Mechanical Properties and Microstructure, *Metall. Mater. Trans. A*, 1994, **25A**, p 789–98
4. C.V. Robino, P.W. Hochanadel, G.R. Edwards and M.J. Cieslak, Heat Treatment of Investment Cast PH 13–8 Mo Stainless Steel: Part II. Isothermal Aging Kinetics, *Metall. Mater. Trans. A*, 1994, **25**, p 697–704
5. R.J. Hamlin and J.N. DuPont, Microstructural Evolution and Mechanical Properties of Simulated Heat-Affected Zones in Cast Precipitation-Hardened Stainless Steels 17-4 and 13-8+Mo, *Metall. Mater. Trans. A*, 2017, **48A**, p 264–364
6. R.J. Hamlin and J.N. DuPont, Influence of Multiple Gleeble-Simulated Weld Thermal Cycles on Maraging 17-4 and 13-8+Mo, *Weld J.*, 2018, **97**, p 253–262
7. R.J. Hamlin, J.N. DuPont and C.V. Robino, Simulation of the Precipitation Kinetics of Maraging Stainless Steels 17-4 and 13-8+Mo During Multi-pass Welding, *Metall. Mater. Trans. A*, 2019, **50**, p 719–732
8. M. Avrami, Kinetics of Phase Change. I: General Theory, *J. Chem. Phys.*, 1939, **7**, p 1103–12
9. M. Avrami, Kinetics of Phase Change. II: Transformation-Time Relations for Random Distribution of Nuclei, *J. Chem. Phys.*, 1940, **8**, p 212–124
10. M. Avrami, Granulation, Phase Change, and Microstructure: Kinetics of Phase Change. III, *J. Chem. Phys.*, 1941, **9**, p 177–84
11. V. Gerold and H. Haberkorn, On the Critical Resolved Shear Stress of Solid Solutions Containing Coherent Precipitates, *Phys. Status Solidi*, 1966, **16**, p 675–684
12. D. Tabor, *The Hardness of Metals*, Oxford University Press, New York, 1951, p 67–76
13. U.K. Viswanathan, P.K.K. Nayar and R. Krishnan, Kinetics of Precipitation in 17-4 PH Stainless Steel, *Mater. Sci. Technol.*, 1989, **5**, p 346–349
14. H. Mirzadeh and A. Najafizadeh, Aging Kinetics of 17-4 PH Stainless Steel, *Mater. Chem. Phys.*, 2009, **116**, p 119–124
15. Y. Asayama, Precipitation and Notch Tensile Strengths of Precipitation Hardening Stainless Steels, *J. Japan Inst. Metals*, 1981, **45**(7), p 731–739
16. J.W. Christian, *Theory of Transformations in Metals and Alloys*, Pergamon Press, Oxford, 2002, p 529–552
17. American Society for Testing and Materials, Standard E140, ASTM International, 2019
18. R.J. Hamlin, "Investigation of Precipitation and Hardening Response of Maraging Stainless Steels 17-4 and 13-8+Mo during Multi-pass Welding," PhD. Thesis, 2017, Bethlehem, PA, pp. 36–100
19. C.V. Robino, Engineering Approximations in Welding: Bridging the Gap between Speculation and Simulation, *Weld. J.*, 2016, **95**, p 1s–16s
20. E.J. Mittemeijer, Analysis of the Kinetics of Phase Transformations, *J. Mat. Sci.*, 1992, **27**, p 3977–3987
21. F. Liu, F. Sommer, C. Bos and E.J. Mittemeijer, Analysis of Solid State Phase Transformation Kinetics: Models and Recipes, *Int. Met. Rev.*, 2007, **52**(4), p 193–212
22. W.D. Callister and D.G. Rethwisch, *Fundamentals of Materials Science and Engineering: An Integrated Approach*, 3rd ed. Wiley, Hoboken, 2007, p 263–270
23. J.W. Christian, *Theory of Transformations in Metals and Alloys*, Pergamon Press, Oxford, 2002, p 718–796
24. D.A. Porter and K.E. Easterling, *Phase Transformations in Metals and Alloys*, 3rd ed. CRC Press, London, 1992, p 265–295
25. E.A. Brandes, *Smithells Metal Reference Book*, 6th ed. Butterworth, London, UK, 1983, p 18–55
26. M.B. Berkenpas, J.A. Barnard, R.V. Ramanujan and H.I. Aaronson, A Critique of Activation Energies for Nucleation Growth and Overall Transformation Kinetics, *Scr. Metall.*, 1986, **20**, p 323–328
27. M.J. Starink, On the Applicability of Isoconversion Methods for Obtaining the Activation Energy of Reactions within a Temperature-Dependent Equilibrium State, *J. Mater. Sci.*, 1997, **32**, p 6505–6512
28. J.W. Christian, *Theory of Transformations in Metals and Alloys*, Pergamon Press, Oxford, 2002, p 422–479